Scaling of ventral hippocampal activity during anxiety

Carlo Cerquetella[1,☆], Camille Gontier[2,3], Thomas Forro[1], Jean-Pascal Pfister[2] and Stéphane Ciocchi[1,☆]

[1]*Laboratory of Systems Neuroscience, Department of Physiology, University of Bern, Bühlplatz 5, 3012 Bern, Switzerland.*

[2]*Theoretical Neuroscience Group, Department of Physiology, University of Bern, Muesmatt 27a, 3012 Bern, Switzerland.*

[3]*Current Address: Rehab Neural Engineering Labs, Department of Physical Medicine and Rehabilitation, University of Pittsburgh, 1622 Locust St, Pittsburgh, PA 15219, USA*

[☆]*corresponding authors: Carlo Cerquetella, Stéphane Ciocchi, Laboratory of Systems Neuroscience, Department of Physiology, University of Bern, Bühlplatz 5, 3012 Bern, Switzerland. Email: carlo.cerquetella@unibe.ch, stephane.ciocchi@unibe.ch*

Short Title:

Scaling of ventral hippocampal activity during anxiety

Keywords:

ventral hippocampus, anxiety, anxiety levels, scaling of neural activity, rate remapping, recruitment of neurons

Abstract

Background

The hippocampus supports a multiplicity of functions, with the dorsal region contributing to memory-related spatial representations, while the ventral hippocampus (vH) is primarily involved in emotional processing. While spatial encoding has been extensively investigated, how the vH activity is tuned to emotional states, e.g. to different anxiety levels, is not well understood.

Methods

We developed an adjustable linear track maze (aLTM) for mice to induce different anxiety levels within the same spatial environment. Through *in vivo* single-unit recordings, optogenetic manipulations, and the application of a convolutional classifier, we examined the changes and causal effects of vH activity at different anxiety levels.

Results

We found that anxiogenic experiences activated the vH and that this activity scaled with increasing anxiety levels within the same spatial environment. We identified two processes that contributed to this scaling of anxiety-related activity: rate remapping and the successive recruitment of neurons. Moreover, optogenetic inhibition of the vH reduced anxiety across different levels, while anxiety-related activity scaling could be decoded using a convolutional classifier.

Conclusions

Our findings position the vH as a critical limbic region that functions as an ‘anxiometer’ by scaling its activity based on perceived anxiety levels. Our discoveries go beyond the traditional theory of cognitive maps in the hippocampus underlying spatial navigation and memory, by identifying hippocampal mechanisms selectively regulating anxiety.

Introduction

Anxiety is an evolutionary highly conserved mental and emotional state, reflecting its crucial role for the survival in perilous situations (1, 2). Anxiety is characterized by the anticipation of possible harmful future events creating an attentional bias towards threatening stimuli (3-5). As anxiety prepares an animal or human to face the challenges of an environment, the level of threat has to be carefully interpreted to support adaptive behavior. An altered perception of negative emotions (6) might contribute to persistent dread and/or chronic anxiety disorders which increasingly pose significant personal and societal burdens (7, 8) affecting more than 300 million people worldwide (WHO). As treatments are available but generic and partially ineffective (9-11), there is an urgent need to understand the neurobiological basis of anxiety in more details. Previous studies have implicated areas of the limbic system including the amygdala, cingulate cortex and the hippocampus in the generation of emotions (12). But, the precise brain region where variations in anxiety levels are represented and computed remains elusive. We hypothesized that the hippocampus could play an important role as it is the key structure involved in learning and compares previously stored information (memories) with the current contextual information to generate cognitive maps (13-15). Along the septotemporal or long axis of the hippocampus, differences in synaptic connectivity and molecular expression have been found, inferring functional subdivisions within the hippocampus (16, 17). An increasing number of studies on functional activity and selective lesions of the vH present evidence from rodents to its homologue in humans (the anterior hippocampus) on the key role of the vH in the processing of threatening stimuli (18-21). In rodents, anxiety has been frequently studied in mazes such the elevated plus maze (EPM) which elicit innate anxiety of height and openness as the animals explore the open compartments of the mazes (22-24). vH anxiety neurons, i.e. pyramidal neurons that are activated in the open arms of the EPM, have been linked to anxiety-related behavior and decisions through the routing of anxiety-related information to the prefrontal cortex (25-27). While place cell activity in the hippocampus has been shown to be modulated by the animal's position within the place field or by the

animal's speed to accurately generate cognitive spatial maps of the environment (28), it is not clear if and how the activity level of anxiety-related neurons is modulated. The precise quantification of emotional states and incentives of animals on an EPM is difficult to assess due to the free exploration and trial-free nature of the task. Furthermore, the specific spatial compartments are inherently linked to the emotional states. Because of such spatial embedding of nonspatial information in many such tasks, there is an ongoing discussion on how much nonspatial information, such as emotions, are actually defined by a spatial framework or can be encoded independently in the hippocampus (29, 30).

To address the nature of anxiety coding in the vH, we developed a new adjustable linear track maze (aLTM) task that could be adjusted gradually and allowed us to impose different anxiety levels to an open compartment within the same spatial environment. With the fully automated aLTM, we were further able to overcome some of the rigidities and difficulties of the EPM allowing us to define clear trials and different anxiety levels while recording and manipulating the activity of neurons in the vH.

Methods and Materials

Subjects

Male C57BL6/J mice aged 4-6 months (Janvier Labs, France) were group housed with *ad libitum* access to food and water in a temperature-controlled room on a 12-hour light/dark cycle. Following surgery, mice were single-housed and recovered for at least 21 days. Behavioral experiments were conducted in the light phase and animals were food deprived to reach 90% and not less than 85% of the baseline weight (= average weight of 3 consecutive days prior to the experiment day). All experimental protocols adhered to the guidelines set forth by the Animal Welfare Office at the University of Bern and received approval from the Veterinary Office of the Canton of Bern.

Surgical procedures

Mice were anesthetized with isoflurane (Attane, Provet, induction 4% in oxygen at a flow rate of 1L/min in anesthetic box, maintenance of the anesthesia based on 1.5-2% of isoflurane in oxygen at a flow rate of 0.8 L/min during the entire surgery) and body temperature was maintained at 37°C with a temperature controller (Harvard Apparatus). Analgesia was administered upon induction and for 3 days post-operation (Carprofen, 2-5 mg/kg subcutaneous). The incision site was infiltrated with lidocaine (2%, Sintetica). Implants were secured to the skull using light-cured dental adhesive (Kerr, OptiBond Universal) and dental cement (Ivoclar, Tetric EvoFlow). After surgery, mice were returned to their home cages for recovery and kept warm for 3 days by warming the cages through a heating pad (Medisana, HP625).

Virus injection and fiber implantation

For optogenetics experiments, mice were infused bilaterally in the vH with the following coordinates: AP: -3.08 mm, ML: ±3 mm, DV: -3.8 mm. The viral solution (250 nL) was delivered via a glass micropipette (30-40 µm tip) attached by tubing to a Picospritzer III microinjection

system (Parker Hannifin Corporation) at a rate of 25 nL/min. Bilateral infusion of either ssAAV5-CamKIIα-eArchT3.0-EYFP or ssAAV5-CamKIIα-EYFP (ETH Zurich Viral Vector Facility) was immediately followed by optic fibers implantation (200 µm core, 0.37 numerical aperture, Thorlabs) above the vH at the following coordinates: AP: -3.08 mm, ML: ±3 mm, DV: -3.75 mm (Figure 2A). The optic fiber implants were fixed to the skull with stainless steel screws, resin-based dental cement (A1 Tetric EvoFlow, Ivoclar Vivadent) and light-cured dental adhesive (Kerr, OptiBond Universal). To ensure sufficient expression of the viral construct a minimum of four weeks was allowed for the animals to recover before conducting the behavioral experiments.

Optogenetic manipulation

For the optogenetic inhibition of CamKIIα^{+} neurons during linear track maze navigation, a continuous light pulse was delivered in the second half of the central compartment (Figure 2C) via a patch cord coupled to a laser beam (Cobolt 06 – DPL 561 nm, Hübner Photonics). The laser was triggered automatically when the animal's body center was detected inside the second half of the central compartment and was turned off as the animal's body center was detected in the openable compartment using the ANY-maze animal tracking software.

Surgery for *in vivo* electrophysiological recordings

Mice were implanted with a custom-made microdrive (Axona Ltd.) containing 8 independently moveable tetrodes made of four gold-plated (NanoZ, Multi Channel Systems) twisted tungsten microwires (12.7 µm inner diameter, California Fine Wire Company, impedances < 150 kΩ). Microdrives were lowered to the vH. Implants were fixed to the skull with 5 miniature stainless steel screws (00-96x1/16, Bilaney) with two of them placed above the cerebellum and connected to the electrode interface board to serve as ground for the electrophysiological recordings.

Adjustable Linear track maze (aLTM)

A home-made adjustable linear track maze (31) (L80 cm x W10-7 cm x H12 cm) was built in order to create 4 different anxiety levels in mice: First, a ‘no anxiety’ (NA, Figure 1A top left) configuration in which the entire maze was surrounded by walls and the mice had to visual insight into the height of the maze. Second, a ‘low anxiety’ (LA, Figure 1A top right) configuration in which the openable second half of the maze was opened and the mice could perceive the 70 cm height of the maze. Third, a ‘moderate anxiety’ (MA, Figure 1A bottom left) configuration where the maze was further elevated by a minilift (ESM100, Dahlgaard & Co.) to 120 cm from the ground. Fourth, the ‘high anxiety’ (HA, Figure 1A bottom right) configuration in which the maze was still at 120 cm height but the open part was changed to a narrower width from 10 cm to 7 cm. 5 mg reward pellets were randomly placed in different locations on the openable part after each trial to motivate the mice. A custom made automatic door (Stepper driver ROB-12859, SparkFun Electronics; Cypress Semiconductor Corp; Switch snap, C&K) in the closed part was built in order to break stereotypic behaviors and create a safe environment for resting in between sessions without any interference from the experimenter (Figure 1A).

The different anxiety configuration were presented consecutively with increasing anxiety (from NA to LA to MA to HA). For each configuration the mouse was first placed into the closed compartment with the door closed for 300 seconds for habituation and rest. Then the door was opened and the mouse was free to initiate a trial or not. If the mouse explored the second half of the maze (the openable compartment) and returned to the closed part the door would be closed for 10-40 seconds. For each configuration the time the mouse could run trials lasted 500 seconds. In a 2 minutes break between each configuration the mice rested in the closed compartment with the door closed. For behavioral and neural recordings including descending levels of anxiety the opposite order of configuration was applied (from HA to MA to LA to NA). In the novel configuration a control NA session would be compared to a ‘novel’ configuration (300s rest + 500s with trials) where the walls in the openable part would be replaced by walls

decorated with stripes of a different color (yellow stripes) and different texture (tape) (Figure 5A right).

For anxiety testing every animal had been used up to 4 times with an interval of at least 5 days between each experiment. Videotaping was carried out from above the maze with the behavior system ANY-maze (www.any-maze.com). Lighting was maintained at 50 lux in each configuration.

Histology

Mice were overdosed with a 5% ketamine and 2.5% xylazine solution (0.02 ml/g) and transcardially perfused with phosphate buffer saline (0.1M PBS, pH 7.4, Roche) followed by 4% paraformaldehyde (PFA, Roti Histofix 4 %, Roth). For electrophysiology experiments, mice were anaesthetized with isoflurane (as stated above) prior to perfusion and electrolytic lesions were made at the tip of each recording tetrode by applying 5 times 30 µA for 2 seconds. Brains were kept in 4% PFA for 24 hours post-fixation. After a rinse in PBS for at least 24 hours at 4°C, brains were sectioned coronally at a thickness of 50 µm using a vibratome (VT1000 S, Leica Microsystems) and preserved in 0.5% sodium azide PBS at 4°C. Lesions were located and only tetrodes positioned in the vH were included for further analysis (Suppl Figure 1).

Immunohistochemistry

Free floating brain slices were blocked with 5 % normal donkey serum (NDS, Abcam) in 0.1% Triton X-100 in PBS (PBS-T) for 30 minutes on a shaker at room temperature (25 °C). Sections were incubated for 72 hours at 4°C with an anti-GFP antibody (1:100, Abcam, ab13970) washed with PBS-T for 5 minutes (3x) and incubated for 2 hours at room with secondary antibody (AlexaFluor-488 1:100, Jackson ImmunoResearch Laboratories, 703545145). Slices were mounted onto slides (ThermoFisher) and coverslipped with aqueous mounting medium (Aqua-Poly-Mount, Polyscience). Sections were imaged on a stereomicroscope (Leica M205 FCA, Leica) mounted with a monochrome camera (Leica DFC345 FX, Leica) and a UV light

source (X-CITE, Lumen Dynamics) or with a confocal microscope (LSM 880, Zeiss, Jena, Germany) and stored at 4°C.

Behavior with electrophysiological recordings

After 21 days post-surgery, the mice were familiarized to the experiment room and acclimated to the handling procedures, which included cable tethering to the recording system. On the following day, tetrodes were lowered by roughly 150 µm while monitoring hippocampal electrophysiological hallmarks (i.e. sharp-wave-ripple and theta oscillations amplitude) and multi-unit spiking activity of the stratum pyramidale was detected. Electrophysiological signals were synchronized to behavior via TTL outputs sent from ANY-maze (at 30 Hertz).

Spike detection and unit classification

The extracellular electrical signals from the tetrodes were amplified, filtered and digitized with a headstage (Intan RHD amplifier, Intan Technologies). The signals were acquired using an Intan RHD2000 evaluation board (Intan Technologies) at a sampling rate of 20 kHz. Neuronal spikes were extracted offline by either using Kilosort2 (32, 33) or by detecting signal amplitudes five standard deviations above the root mean square of the digitally filtered signal (0.8 - 5 kHz) over 0.2 ms sliding windows. A principal component analysis was implemented to extract the first three components of spike waveforms of each tetrode wire (34, 35). Spike waveforms were automatically clustered using KlustaKwik (http://klustakwik.sourceforge.net/). Individual units were manually refined in Klusters (36).

Computational methods

Calculations were performed on UBELIX (http://www.id.unibe.ch/hpc), the HPC cluster at the University of Bern. For quantification performed on neuronal populations, z-scored neuronal activities were calculated to allow unbiased comparisons of firing rates. Each neuron was independently z-scored based on its activity in the entire recording session. To account and correct for a correlation between speed and neuronal activity a generalised linear model (GLM) of the z-scored neuronal activity was fitted in MATLAB (glmfit function) for neurons that were

significantly speed correlated (Pearson's r with $p < 0.05$). Moreover, to assess the influence of the configuration, animal position and speed on the firing rate of neurons, we fitted seven different GLMs with different variable combinations. Their goodness-of-fit were compared using the BIC criterion (Vrieze, 2012).

Decoding was performed using the ResNet18 architecture (37) distributed as part of PyTorch (38). Networks were trained using a cross-entropy loss with the ADAM optimizer (39) with the following parameters:

Learning rate $\gamma=0.01$

Weight decay parameter $\lambda=0.0025$

Dropout probability $p=0.1$

Ratio of training data to training and validation data: 70%

Number of epochs: 100

Batch size: 150

N = 25

For each training or test sample, the input to the network is an m*N matrix, where m is the number of recorded neurons in the session.

Statistical analysis

Analyses were conducted in GraphPad PRISM and MATLAB using custom scripts. All datasets were tested for normality using the D'Agostino & Pearson test, and if found to be normally distributed, we used parametric tests or otherwise the equivalent non-parametric tests. In case of multiple comparison, significance was evaluated with a one-way or two-way repeated measures ANOVA or Friedman's test followed by Tukey's, Dunn's or Uncorrected Fisher's LSD post hoc tests. Significance in proportions was assessed by Chi-square test.

Data availability

The datasets generated during the current study are available from the corresponding authors upon request.

Results

A novel linear track maze to induce scaling of anxiety behaviour

Our novel adjustable linear track maze (aLTM) allows to induce 4 different levels of anxiety in 6 mice. To achieve this, the maze consists of a closed and openable part, could be placed at 70 cm or 120 cm height and the floor width of the openable part could be changed from 10 cm to 7 cm (Figure 1A, Methods and Materials). This allowed us to compare 4 different anxiety levels: a ‘no anxiety’ (NA), a ‘low anxiety’ (LA), a ‘moderate anxiety’ (MA), and a ‘high anxiety’ (HA) configuration which were presented to the mice successively (Figure 1A). In each configuration, food-restricted mice could engage in running trials for 500 seconds to the openable compartment to consume a small reward (sugar pellet). We assessed the level of anxiety by evaluating the percentage of time that the mice spent in the openable part and by quantifying the number of trials performed to the openable part.

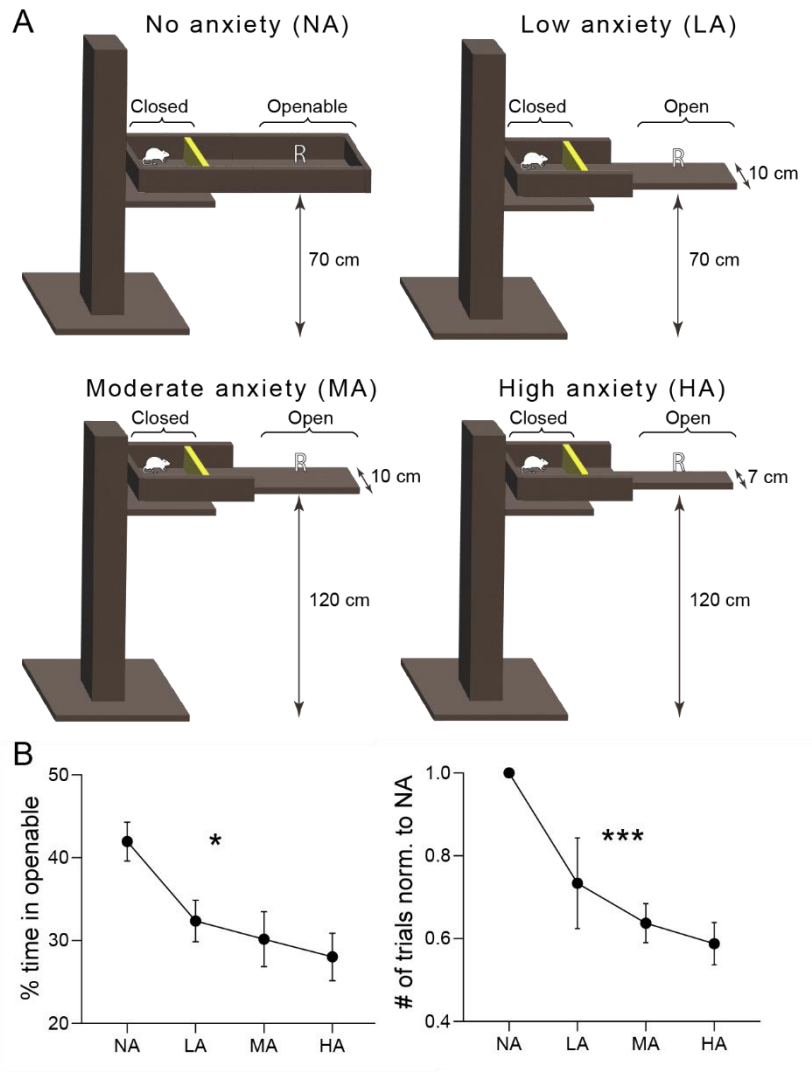

Figure 1. Different configurations of the aLTM induce increasing levels of anxiety behavior. (A) NA to LA to MA to HA configurations were presented successively. The yellow rectangle in the maze represents an automated door that closed after each trial for a random amount of time (between 10-40 seconds). The 'closed' part was defined as the space up to the door and the 'openable/open' part started when the whole body of the mice entered the open space (defined as 2cm into the open space). 'R' indicates that the reward was given in the openable/open part of the maze at changing positions. **(B)** Percentage of time (right) the animals spent in the openable and number of trials (left) performed in all configurations indicate gradually increasing anxiety from NA to HA. Left, Friedman test $p = 0.017$, $r = -0.36$ with $p < 0.001$ Spearman correlation, N = 6 animals. Right, Friedman test $p < 0.001$, $r = -0.55$

with $p < 0.001$ Spearman correlation, N = 6 animals, n = 22 experimental days. All post hoc test results in supplementary table 1 and supplementary table 2. Error bars represent ± SEM.

In classical anxiety tests such as the EPM, a reduced time spent in and fewer entries to the open arms compared to the closed arms have been shown to be related to higher anxiety in the open arms (24, 40). In our task, we found a progressive reduction in the time spent within the open part as the anxiety levels increased (Figure 1B, left) confirming that our anxiety configurations were inducing increasing anxiety in the open part of the maze. We further quantified the number of trials, corresponding to the number of full entries to the open part, showing also a progressive decrease in trials from LA to HA configurations (Figure 1B, right).

vH inhibition reduces and disrupts the scaling of anxiety behaviour

Inhibition of vH activity has been shown to reduce anxiety behavior (41-43). To explore the impact of vH activity in our novel aLTM, we applied an ArchT-mediated optogenetic bilateral intervention in vH CamKIIα^{+} neurons (thereby targeting excitatory pyramidal neurons) during the approach of mice from the closed to the open part of the maze (Figure 2, Methods and Materials). This led to a significant increase of trials and increased time in the open part in the ArchT group of mice across anxiety inducing configurations compared to the control mice (Figure 2). This suggests that vH inhibition reduced anxiety as measured by the entries and time spent in the anxiogenic compartment of the aLTM. Moreover, inhibition of the vH during approach of the open part disrupted the scaling of anxiety approach behavior expressed by unchanging trials number across anxiety levels (Figure 2), indicating that interference with vH activity can disrupt the precise interpretation of a potential threat.

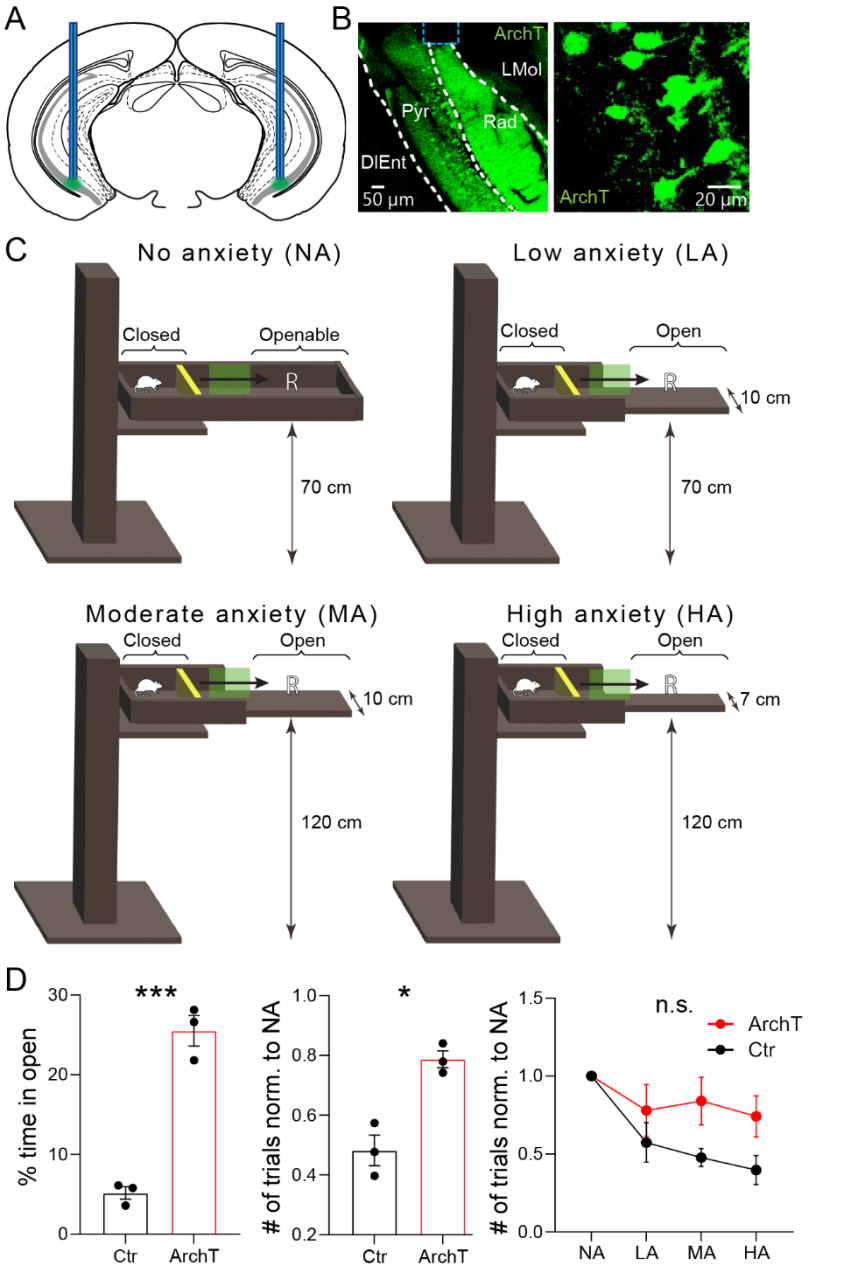

Figure 2. Reduced anxiety-related behavior upon vH inhibition. (A) Schematic representation of injection sites (green circles) of the adeno-associated virus (AAV5) expressing ArchT and eYFP reporter under the control of CamKIIα promoter and optic fiber implants (blue rectangles). **(B)** Anti-YFP immunolabelling of the reporter gene in vH of ArchT mice and a magnified image on the right of putative ventral CA1 pyramidal somata. DlEnt: dorsolateral entorhinal cortex; Pyr: Stratum pyramidale; Rad: Stratum radiatum; LMol: Stratum lacunosum-moleculare; Dashed blue line: optic fiber **(C)** Schematic representation of optogenetic manipulation in outbound trajectories indicating with a green rectangle the start of

light application when the animals reach halfway from the door position to the open space and ending when the mice fully entered the open space. **(D)** ArchT mice (N = 3) spent significantly more time in the open part than eYFP control mice (N = 3) (left, Welch's test $p<0.001$) and ran more trials to the open part of the maze across anxiety configuration (middle, Mann-Whitney test $p = 0.014$). Dots on top of bars represent the 3 anxiety inducing configurations. Right, gradually decreasing scaling of trials taken to the open part was disrupted in ArchT mice but not control mice ($r = -0.59$ and $p < 0.001$ and Ctr, $r = -0.26$ and $p = 0.07$ for ArchT Spearman correlation, Two-way RM ANOVA Row Interaction values: $F = 12.17$, $p = 0.075$ for interaction of configuration with group (ArchT/Ctr). All post hoc test results in supplementary table 3. n = 12 experimental days. Error bars represent ± SEM.

vH activity scales with increasing anxiety levels

Tetrode implantations within the vH enabled the recording of 207 single-units as mice navigated through various anxiety configurations on the aLTM (Suppl. Figure 1). Previous studies have shown that the vH exhibits increased activity in open compartments of mazes (25, 26, 44). Here, we showed that individual neurons and vH population activity not only increased their activity in the open anxiogenic compartments, but that the activity progressively increased from low to high anxiety configurations in the openable part of the maze (Figure 3). This was not due to habituation, passing of time or related to changes in speed of the mice as we showed that vH activity also scaled down during the 'descending' anxiety configurations and that the scaling of activity was not affected when taking account of speed's effect on the neuronal activity using a GLM model (Suppl. Figure 2,3).

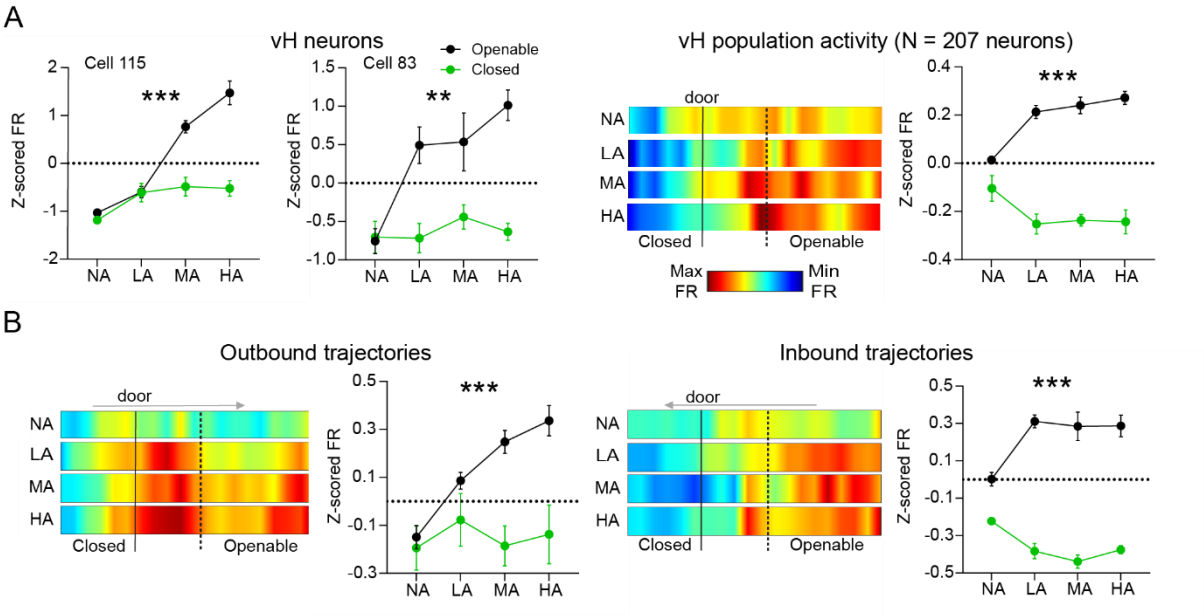

Figure 3. Scaling of vH activity during anxiety. (A) Left, individual example neurons with increasing Z-scored activity in the open compartment across anxiety levels (Cell 115: Two-way RM ANOVA Interaction values: F = 20.12, p < 0.001, r = 0.65 and p = 0.002 for closed and r = 0.9184 and p < 0.001 for open, Spearman correlation. Cell 83: Two-way RM ANOVA Interaction values: F = 6.22, p = 0.002, r = 0.186 and p = 0.43 for closed and r = 0.672 and p < 0.001 for open, Spearman correlation. All post hoc test results in supplementary table 4 and supplementary table 5). Right, heatmaps and Z-scored firing rates show vH population activity progressively increasing in the open part compared to the closed part (Two-way RM ANOVA Interaction values: F = 25.71, p < 0.001. All post hoc test results in supplementary table 6, r = -0.349 and p = 0.132 for closed and r = 0.698 and p < 0.001 for open, Spearman correlation. Heat maps depict the linearized firing rate activity of the entire recorded population (n = 207, N = 6 animals, n = 22 experimental days). **(B)** Heatmaps and Z-scored firing rates separated into outbound (left) and inbound trajectories (right) showing gradually scaling during outbound and switching of activity respectively. Left, Two-way RM ANOVA Interaction values: F = 12.77, p < 0.001, r = 0.023 and p = 0.920 for closed and r = 0.82 and p < 0.001, Spearman correlation. Right, two-way RM ANOVA Interaction values: F = 10.78, p < 0.001, r = -0.54 and p = 0.013 for closed and r = 0.43 and p = 0.009, Spearman correlation. All post hoc test results in

supplementary table 7 and supplementary table 8. N = 207 cells, n = 10999 trials. Error bars represent ± SEM.

Rate remapping and recruitment of neurons drive vH scaling during anxiety

What processes in the vH could contribute to the increased activity that we observed? We hypothesized that two phenomena that have been previously described in the hippocampus could contribute: rate remapping and recruitment of additional neurons (45). Rate remapping has been initially described for place cells and refers to a change in firing rate although the position of the expressed place field does not change (46). To reveal if such a process might be also occurring during the scaled representation of anxiogenic information, we selected neurons that significantly increased their activity at each level, i.e. from NA to LA, from LA to MA and from MA to HA, in the open part of the maze. We found 50 neurons (24%) whose firing rates remapped consecutively across the anxiety levels (Figure 4A).

When we looked at the number of neurons that were significantly more activated in the open part, we observed that at each level the number of open-activated neurons (anxiety neurons) increased and was also scaling (Figure 4B). Based on this finding, we hypothesized that the recruitment of new neurons might also play a role in activity scaling. At each level, we investigated the number of neurons that were newly recruited with a significant increase in activity in the openable part compared to the previous level. Our results suggest that at each anxiety level, new neurons were recruited (Figure 4C). Of note, at the population level, the newly recruited neurons did not further increase their activity in subsequent configurations but retained their increased activity.

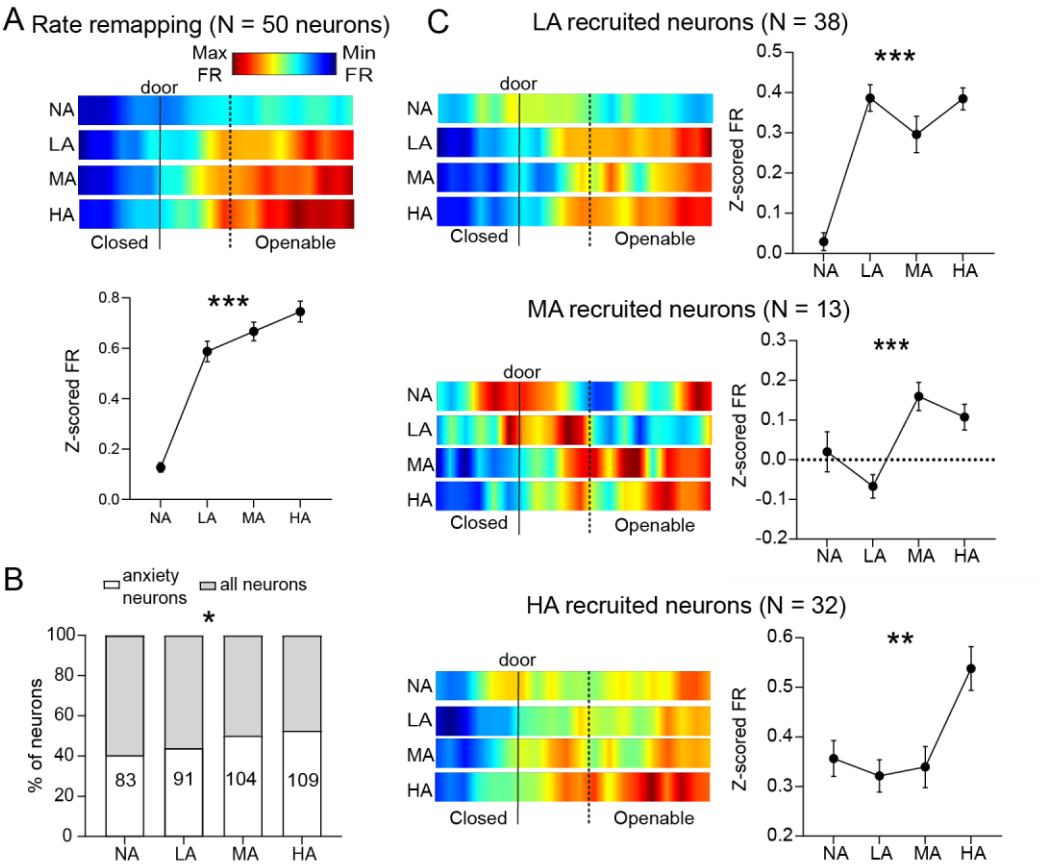

Figure 4. Rate remapping and recruitment of neurons drive vH scaling during anxiety. **(A)** Linearized firing rate heat maps of all cells showing rate remapping mechanism in all configurations and below the quantified Z-scored firing rate activity in the openable compartment. RM one-way ANOVA F = 112.10, $p < 0.001$. All post hoc test results in supplementary table 9, r = 0.79 and $p < 0.001$, Spearman correlation. N = 22 experimental days, n = 50 cells. **(B)** Number and proportions of neurons that were significantly more activated in the openable/open part compared the closed part is increasing across anxiety levels (Chi-square p = 0.041, $X^2 = 8.24$ for change of proportions). **(C)** Heatmaps of linearized firing rates and Z-scored firing rates show sudden switch of activity and persistence of activity of newly recruited cells in LA, MA and HA configurations. RM one-way ANOVA F = 30.18, $p < 0.001$. RM one-way ANOVA F = 9.61, $p < 0.001$. RM one-way ANOVA F = 9.42, p = 0.002. All post hoc test results in supplementary table 10 and supplementary table 11 and supplementary table 12. Error bars represent ± SEM.

Novelty does not change vH population activity

To discern changes induced by novelty from the changes related to anxiety configurations, we replaced the openable compartment with a novel compartment where the sidewalls had a clearly different visual appearance and a different texture (Figure 5A, right). During the exploration of the 'novel configuration', mice demonstrated a heightened preference for the novel section of the maze (Figure 5B, left), but showed no difference in trials undertaken compared to control configuration (corresponding to a NA configuration, Figure 5B, right). This shows that mice expressed a similar motivation to run trials and were able to detect and engage with the novel part of the maze (47).

Novelty can induce a spatial remapping of activity in the hippocampus (46, 48), but we observed that the novelty in the openable compartment did not lead to an increased vH activity compared to the control configuration (corresponding to NA configuration, Figure 5C).

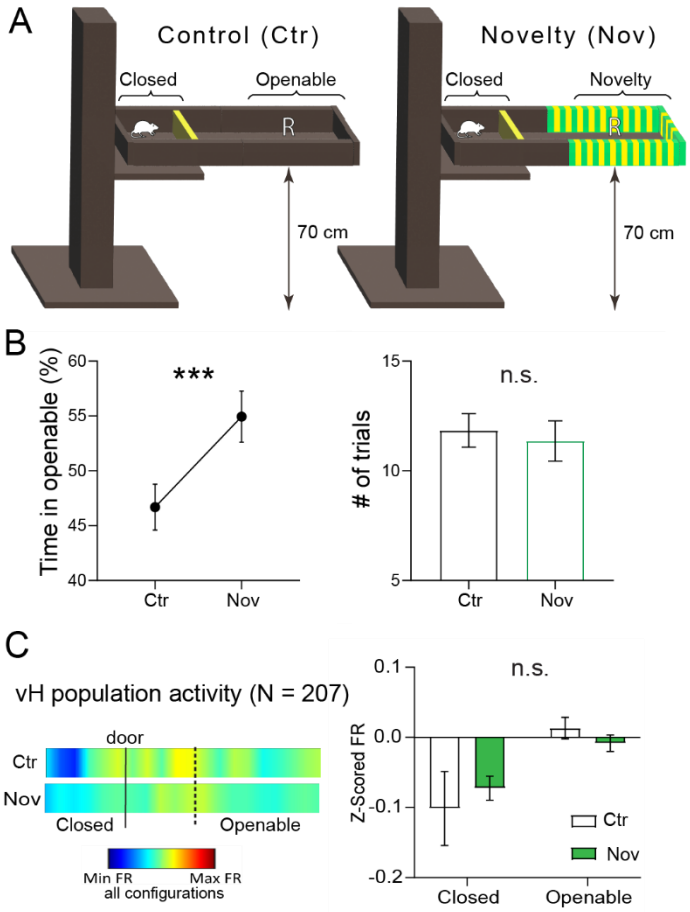

Figure 5. Novelty does not change vH population activity. (A) Control (left) and 'Novelty' (right) configuration representations of the aLTM illustrating the visual differences of the novelty part of the maze. **(B)** Mice spent more time in the novel part of the maze but did not engage in more or less trials than in the control configuration. Wilcoxon test, $p < 0.001$. Paired t-test $p = 0.392$. **(C)** Linearized firing rate heatmaps and Z-scored firing rate shows no significant changes induced by the novelty and that activity levels did not reach values close to the maximum vH activations of the anxiety configurations. Two-way RM ANOVA Interaction values: $F = 1.68$, $p = 0.219$. All post hoc test results in supplementary table 13. N = 207 neurons, n = 22 recordings. Error bars represent ± SEM.

Decoding of anxiety levels by a convolutional classifier confirms the scaling of anxiety-related information

Finally, we trained a convolutional classifier to decode anxiety levels based on vH activity, using as inputs the recorded firing rates from time t-N to t (where N is a fixed lag parameter) (Figure 6). Since different neurons are recorded during each experiment, a different network has been trained for each experiment. The classifier was trained to solely discriminate "NA" and "HA" samples and its validation accuracy was assessed on held-out data (Figure 6B, first and last column). The leftmost column indicated the proportion of "NA" samples which were correctly classified as "NA" configurations. Similarly, the rightmost column indicates the proportion of "HA" samples which were classified as "NA" configuration. Expectedly, this yielded to a converse classification accuracy. Then, we assessed how unseen "LA" and "MA" samples would be sorted by the classifier only trained on "NA" and "HA" samples (Figure 6B, second and third columns). Overall, "LA" samples have a higher probability of being classified as "NA" as compared to "MA" samples, which highlights a closer proximity between the "LA" and "NA" configurations than between "MA" and "NA". Moreover, both "LA" and "MA" test samples are more likely to be classified as "HA" rather than "NA", which hints at a qualitative difference between the "NA" configuration and all the other configurations with an inherent

higher anxiety. Collectively, these results showed that different anxiety levels can be successfully discriminated based on recorded neuronal activity.

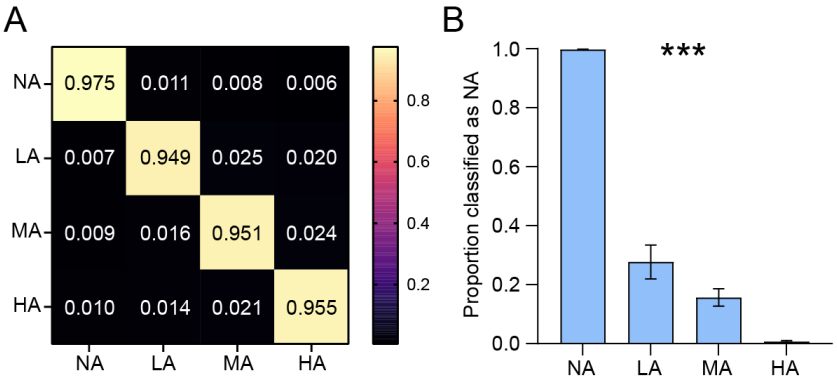

Figure 6. Decoding of anxiety levels by a convolutional classifier. (A) Confusion matrix indicating the validation accuracy. **(B)** Convolutional classifier trained on “NA” and “HA” conditions for each experiment: held-out data for these conditions are used as a validation set (columns 1 and 4) and shows that “NA” and “HA” samples are correctly classified. The test set consists of all data from the “LA” and “MA” conditions (columns 2 and 3). Results show that the decoder output continuously varies with the different anxiety levels. X-axis: ground-truth labels. Y-axis: probability of being classified as “NA” configuration. Results are averaged over 12 experiments. Friedman test $p < 0.001$. All post hoc test results in supplementary table 14. Error bars represent ± SEM.

Discussion

Humans and animals must strike a balance between minimizing exposure to possibly harmful events and seeking needs that maximize well-being. Anxiety has been suggested to bias decision-making by increasing the prediction of negative future outcomes (49, 50). However, how anxiety coding in the brain is involved in risk assessment to guide behavior is not yet well understood. In our study, we investigated how anxiety representations in the vH of mice are tuned to different levels of anxiety and might thereby provide a basis for decisions under negative emotional conflict. For this, we developed a new maze, the aLTM, on which mice could be exposed to 4 different anxiety levels during navigation in the same spatial environment while we recorded the activity of vH neurons.

We found that we could successfully induce different levels of anxiety behavior in mice and that the vH activity progressively scaled with the different anxiety levels. Human neuroimaging studies have shown that greater hippocampal BOLD signals in the anterior hippocampus are associated with a greater probability of threat and higher anxiety during emotional conflicts and safety learning (20, 51). With our results, we showed that vH activity did not simply change in an all-or-none manner during anxiety, but rather finely tunes and scales with different anxiety levels, suggesting that the vH might act as an ‘anxiometer’ in the brain. Previous work has shown that the basal amygdala encodes behavioral states such as freezing, head dips, entries and exits to anxiogenic compartments, but does not represent the level of absolute perceived anxiety (52). Rather, our findings position the vH as a critical limbic region that functions as an ‘anxiometer’ by scaling its activity based on perceived anxiety levels. To test the causal relationship between the scaling vH activity and anxiety experienced by the animals, we applied ArchT-mediated optogenetic intervention during the approach of the open compartment of the maze. In a study in humans, the decision to approach a reward relied on the hippocampus and not on the amygdala (19). In line with this finding, when we inhibited the vH during the approach of the open anxiogenic environment, the mice expressed reduced anxiety and a disruption in the scaling anxiety behaviour in the open part of the maze. Hence,

we posit that vH activity plays a crucial role not only in the generation of anxiety representations (53, 54), but our findings further substantiate that activity associated with anxiety, in particular when facing anxiogenic situations (i.e. corresponding to outbound trajectories when approaching the anxiogenic compartment) may instruct downstream decision-making areas to perform risk assessment.

Tuning of neuronal activity has been extensively described in sensory areas, for example, in orientation-tuned neurons in the primary visual cortex that fire with the highest activity to specific orientation of a visual stimulus (55, 56). Responses of dopamine neurons in the ventral tegmental area of the midbrain have been also described to scale to error prediction depending on reward size (57). The integration of sensory stimuli such as odors, tones or speed of the animal have been shown in the hippocampus and entorhinal cortex to drive neural activity levels (58-61). How might individual neurons and population codes in higher cognitive areas such as the hippocampus achieve a tuning to internally generated emotional states such as anxiety? We described two processes that contributed to the scaling of anxiety-related activity in the vH, i.e. a rate remapping and recruitment of additional neurons. The concept of remapping has been well described in the hippocampus and relies on a spatial framework whereby neurons can either change their firing rates in the same location referred to as rate remapping or in a new environment randomly reconfigure spatial codes during global remapping (62). We argue that these processes might not be restricted to the encoding of space but to any information that is predominantly processed by the underlying hippocampal subregion (63). The recruitment of new vH neurons that were activated at higher anxiety levels might reflect a process similar to global remapping whereby neurons that were not responding in previous anxiety encounters were engaged and recruited at a specific anxiety ‘threshold’, not to a new environment as during global remapping, but to a different anxiety level. vH circuits integrate a multiplicity of synaptic inputs: e.g. visual-spatial contexts and object information from the medial and lateral entorhinal cortex and anxiety-related information from the basolateral amygdala (42, 64, 65). We speculate that convergence of synaptic inputs and

possibly inhibitory microcircuits might tune the scaling of rate remapping populations and gate the switching of newly recruited neurons during different anxiety encounters.

All changes of the anxiety configurations happened within the same spatial environment but the changes even if small were of physical nature (e.g. distance to the ground or removal or part of the maze floor). To exclude that the mice might perceive these as novel aspects of the environment, we introduced a novel configuration of the maze. Based on our results, we conclude that even if a remapping has occurred, it did not result in such a prominent dynamic increase of activity as observed across anxiety configurations and therefore novelty is unlikely to have driven the observed changes.

Anxiety disorders in humans are characterized by an elevated perception of potential threats leading to excessive uncontrollable worries that patients overcome with difficulties (66, 67). In patients with obsessive-compulsive disorders (a form of generalized anxiety) and schizophrenia (with frequent emotional disturbances), hyperactivity of the vH has been reported (68, 69). Also, patients with temporal lobe epilepsy and hyperexcitability of the vH can experience anxiety disorders (69, 70). We hypothesize that in some of these patients the mechanisms to control and adjust the scaling of vH activity may be dysfunctional, possibly either shifted to more elevated levels or instead of gradually scaling rather jump to higher levels and thereby patients are experiencing inappropriate anxiety to guide their decisions and behavior. Collectively, our findings provide insight into how the hippocampus could allow for a dynamic and flexible adjustment of anxiety responses according to accumulated experience and prevailing environmental conditions. These processes, when disrupted, may contribute to the manifestation of anxiety disorders.

Acknowledgments

This work was supported by the following grants: an ERC starting grant (716761) to S.C., a Swiss National Science Foundation professorship grant (170654) to S.C., a Swiss National Science Foundation grant (31003A_175644) to J.P.P, and a Swiss National Science Foundation grant (P500PM_210800) to C.G.. C.C. and S.C. designed the experiments. C.C. performed experiments and data analysis. C.C., S.C. and T.F. interpreted the data, prepared and wrote the manuscript. C.G. and J.P.P contributed to data analysis and edited the manuscript. We further thank Kaizhen Li for the help with histology and immunolabelling, the electronic workshop and members of the Ciocchi Laboratory for their valuable inputs on the project. We thank Jakob Jordan and Nicolas Deperrois for fruitful discussions.

Disclosures

The authors declare no competing interests.

References

1. Koskinen MK, Hovatta I (2023): Genetic insights into the neurobiology of anxiety. *Trends Neurosci*. 46:318-331.

2. Sylvers P, Lilienfeld SO, LaPrairie JL (2011): Differences between trait fear and trait anxiety: Implications for psychopathology. *Clin Psychol Rev*. 31:122-137.

3. Miceli M, Castelfranchi C (2015): *Expectancy and emotion*. Oxford: Oxford University Press.

4. Parfitt GM, Nguyen R, Bang JY, Aqrabawi AJ, Tran MM, Seo DK, et al. (2017): Bidirectional Control of Anxiety-Related Behaviors in Mice: Role of Inputs Arising from the Ventral Hippocampus to the Lateral Septum and Medial Prefrontal Cortex. *Neuropsychopharmacol*. 42:1715-1728.

5. Baldwin DS, Allgulander C, Bandelow B, Ferre F, Pallanti S (2010): Treatment of Generalized Anxiety Disorder in Routine Clinical Practice: An International Survey. *J Psychopharmacol*. 24:A71-A71.

6. Feldborg M, Lee NA, Hung K, Peng K, Sui J (2021): Perceiving the Self and Emotions with an Anxious Mind: Evidence from an Implicit Perceptual Task. *Int J Environ Res Public Health*. 18.

7. Di Luca M, Baker M, Corradetti R, Kettenmann H, Mendlewicz J, Olesen J, et al. (2011): Consensus document on European brain research. *Eur J Neurosci*. 33:768-818.

8. Kavelaars R, Ward H, Mackie DS, Modi KM, Mohandas A (2023): The burden of anxiety among a nationally representative US adult population. *J Affect Disorders*. 336:81-91.

9. Ansara ED (2020): Management of treatment-resistant generalized anxiety disorder. *Ment Health Clin*. 10:326-334.

10. Garakani A, Murrough JW, Freire RC, Thom RP, Larkin K, Buono FD, et al. (2020): Pharmacotherapy of Anxiety Disorders: Current and Emerging Treatment Options. *Front Psychiatry*. 11:595584.

11. Bandelow B, Michaelis S, Wedekind D (2017): Treatment of anxiety disorders. *Dialogues Clin Neuro*. 19:93-106.

12. Shin LM, Liberzon I (2010): The neurocircuitry of fear, stress, and anxiety disorders. *Neuropsychopharmacology*. 35:169-191.

13. Nomoto M, Murayama E, Ohno S, Okubo-Suzuki R, Muramatsu S, Inokuchi K (2022): Hippocampus as a sorter and reverberatory integrator of sensory inputs. *Nat Commun*. 13.

14. Duncan K, Ketz N, Inati SJ, Davachi L (2012): Evidence for area CA1 as a match/mismatch detector: A high-resolution fMRI study of the human hippocampus. *Hippocampus*. 22:389-398.

15. Katz Y, Kath WL, Spruston N, Hasselmo ME (2007): Coincidence detection of place and temporal context in a network model of spiking hippocampal neurons. *PLoS Comput Biol*. 3:e234.

16. Cenquizca LA, Swanson LW (2007): Spatial organization of direct hippocampal field CA1 axonal projections to the rest of the cerebral cortex. *Brain Res Rev*. 56:1-26.

17. Fanselow MS, Dong HW (2010): Are the dorsal and ventral hippocampus functionally distinct structures? *Neuron*. 65:7-19.

18. Bannerman DM, Grubb M, Deacon RM, Yee BK, Feldon J, Rawlins JN (2003): Ventral hippocampal lesions affect anxiety but not spatial learning. *Behav Brain Res*. 139:197-213.

19. Bach DR, Hoffmann M, Finke C, Hurlemann R, Ploner CJ (2019): Disentangling Hippocampal and Amygdala Contribution to Human Anxiety-Like Behavior. *J Neurosci*. 39:8517-8526.

20. Bach DR, Guitart-Masip M, Packard PA, Miro J, Falip M, Fuentemilla L, et al. (2014): Human Hippocampus Arbitrates Approach-Avoidance Conflict. *Curr Biol*. 24:1435.

21. Ito R, Lee ACH (2016): The role of the hippocampus in approach-avoidance conflict decision-making: Evidence from rodent and human studies. *Behav Brain Res*. 313:345-357.

22. Cryan JF, Holmes A (2005): The ascent of mouse: advances in modelling human depression and anxiety. *Nat Rev Drug Discov*. 4:775-790.

23. Rodgers RJ, Cao BJ, Dalvi A, Holmes A (1997): Animal models of anxiety: an ethological perspective. *Braz J Med Biol Res*. 30:289-304.

24. Carobrez AP, Bertoglio LJ (2005): Ethological and temporal analyses of anxiety-like behavior: the elevated plus-maze model 20 years on. *Neurosci Biobehav Rev*. 29:1193-1205.

25. Jimenez JC, Su K, Goldberg AR, Luna VM, Biane JS, Ordek G, et al. (2018): Anxiety Cells in a Hippocampal-Hypothalamic Circuit. *Neuron*. 97:670-683 e676.

26. Ciocchi S, Passecker J, Malagon-Vina H, Mikus N, Klausberger T (2015): Brain computation. Selective information routing by ventral hippocampal CA1 projection neurons. *Science*. 348:560-563.

27. Adhikari A, Topiwala MA, Gordon JA (2010): Synchronized Activity between the Ventral Hippocampus and the Medial Prefrontal Cortex during Anxiety. *Neuron*. 65:257-269.

28. Geisler C, Robbe D, Zugaro M, Sirota A, Buzsaki G (2007): Hippocampal place cell assemblies are speed-controlled oscillators. *Proc Natl Acad Sci U S A*. 104:8149-8154.

29. O'Keefe J, Krupic J (2021): Do Hippocampal Pyramidal Cells Respond to Nonspatial Stimuli? *Physiol Rev*. 101:1427-1456.

30. Lisman J, Buzsáki G, Eichenbaum H, Nadel L, Rangananth C, Redish AD (2017): Viewpoints: how the hippocampus contributes to memory, navigation and cognition. *Nat Neurosci*. 20:1434-1447.

31. Malagon-Vina H, Ciocchi S, Klausberger T (2023): Firing patterns of ventral hippocampal neurons predict the exploration of anxiogenic locations. *Elife*. 12.

32. Pachitariu M, Steinmetz N, Kadir S, Carandini M, Harris K (2016): Fast and accurate spike sorting of high-channel count probes with KiloSort. *Adv Neur In*. 29.

33. Stringer C, Pachitariu M, Steinmetz N, Reddy CB, Carandini M, Harris KD (2019): Spontaneous behaviors drive multidimensional, brainwide activity. *Science*. 364:255.

34. Harris KD, Henze DA, Csicsvari J, Hirase H, Buzsaki G (2000): Accuracy of tetrode spike separation as determined by simultaneous intracellular and extracellular measurements. *J Neurophysiol*. 84:401-414.

35. Henze DA, Borhegyi Z, Csicsvari J, Mamiya A, Harris KD, Buzsaki G (2000): Intracellular features predicted by extracellular recordings in the hippocampus in vivo. *J Neurophysiol*. 84:390-400.

36. Hazan L, Zugaro M, Buzsaki G (2006): Klusters, NeuroScope, NDManager: a free software suite for neurophysiological data processing and visualization. *J Neurosci Methods*. 155:207-216.

37. He KM, Zhang XY, Ren SQ, Sun J (2016): Deep Residual Learning for Image Recognition. *Proc Cvpr Ieee*.770-778.

38. Paszke A, Gross S, Massa F, Lerer A, Bradbury J, Chanan G, et al. (2019): PyTorch: An Imperative Style, High-Performance Deep Learning Library. *Advances in Neural Information Processing Systems 32 (Nips 2019)*. 32.

39. Kingma DPB, J. (2017): Adam: A Method for Stochastic Optimization. In: arXiv, editor. *3rd International Conference for Learning Representations*. San Diego.

40. Poulton R, Menzies RG (2002): Non-associative fear acquisition: a review of the evidence from retrospective and longitudinal research. *Behav Res Ther*. 40:127-149.

41. Padilla-Coreano N, Bolkan SS, Pierce GM, Blackman DR, Hardin WD, Garcia-Garcia AL, et al. (2016): Direct Ventral Hippocampal-Prefrontal Input Is Required for Anxiety-Related Neural Activity and Behavior. *Neuron*. 89:857-866.

42. Maestas-Olguin C, Fennelly JW, Pentkowski NS (2021): Chemogenetic inhibition of ventral hippocampal CaMKIIalpha-expressing neurons attenuates anxiety- but not fear-like defensive behaviors in male Long-Evans hooded rats. *Neurosci Lett*. 751:135777.

43. Zhang WN, Bast T, Xu Y, Feldon J (2014): Temporary inhibition of dorsal or ventral hippocampus by muscimol: Distinct effects on measures of innate anxiety on the elevated plus maze, but similar disruption of contextual fear conditioning. *Behav Brain Res*. 262:47-56.

44. Forro T, Volitaki E, Malagon-Vina H, Klausberger T, Nevian T, Ciocchi S (2022): Anxiety-related activity of ventral hippocampal interneurons. *Prog Neurobiol*. 219:102368.

45. Colgin LL, Moser EI, Moser MB (2008): Understanding memory through hippocampal remapping. *Trends Neurosci*. 31:469-477.

46. Leutgeb S, Letugeb JK, Barnes CA, Moser EI, McNaughton BL, Moser MB (2005): Independent codes for spatial and episodic memory in hippocampal neuronal ensembles. *Science*. 309:619-623.

47. File SE (2001): Factors controlling measures of anxiety and responses to novelty in the mouse. *Behav Brain Res*. 125:151-157.

48. Dong C, Madar AD, Sheffield MEJ (2021): Distinct place cell dynamics in CA1 and CA3 encode experience in new environments. *Nat Commun*. 12.

49. Gagne C, Dayan P, Bishop SJ (2018): When planning to survive goes wrong: predicting the future and replaying the past in anxiety and PTSD. *Curr Opin Behav Sci*. 24:89-95.

50. Hartley CA, Phelps EA (2012): Anxiety and decision-making. *Biol Psychiatry*. 72:113-118.

51. Odriozola P, Kribakaran S, Cohodes EM, Zacharek SJ, McCauley S, Haberman JT, et al. (2023): Hippocampal Involvement in Safety Signal Learning Varies With Anxiety Among Healthy Adults. *Biological Psychiatry Global Open Science*.

52. Grundemann J, Bitterman Y, Lu T, Krabbe S, Grewe BF, Schnitzer MJ, et al. (2019): Amygdala ensembles encode behavioral states. *Science*. 364.

53. Eysenck MW, Derakshan N (2011): New perspectives in attentional control theory. *Pers Indiv Differ*. 50:955-960.

54. Moser JS, Becker MW, Moran TP (2012): Enhanced attentional capture in trait anxiety. *Emotion*. 12:213-216.

55. Hubel DH, Wiesel TN (1962): Receptive fields, binocular interaction and functional architecture in the cat's visual cortex. *J Physiol*. 160:106-154.

56. Niell CM, Stryker MP (2008): Highly selective receptive fields in mouse visual cortex. *Journal of Neuroscience*. 28:7520-7536.

57. Eshel N, Tian J, Bukwich M, Uchida N (2016): Dopamine neurons share common response function for reward prediction error. *Nat Neurosci*. 19:479-486.

58. Aronov D, Nevers R, Tank DW (2017): Mapping of a non-spatial dimension by the hippocampal-entorhinal circuit. *Nature*. 543:719-+.

59. Aikath D, Weible AP, Rowland DC, Kentros CG (2014): Role of Self-Generated Odor Cues in Contextual Representation. *Hippocampus*. 24:1039-1051.

60. Iwase M, Kitanishi T, Mizuseki K (2020): Cell type, sub-region, and layer-specific speed representation in the hippocampal-entorhinal circuit. *Sci Rep-Uk*. 10.

61. Kropff E, Carmichael JE, Moser MB, Moser EI (2015): Speed cells in the medial entorhinal cortex. *Nature*. 523:419-U478.

62. Schlesiger MI, Boublil BL, Hales JB, Leutgeb JK, Leutgeb S (2018): Hippocampal Global Remapping Can Occur without Input from the Medial Entorhinal Cortex. *Cell Rep*. 22:3152-3159.

63. Eichenbaum H (2018): What Versus Where: Non-spatial Aspects of Memory Representation by the Hippocampus. *Curr Top Behav Neurosci*. 37:101-117.

64. Felix-Ortiz AC, Beyeler A, Seo C, Leppla CA, Wildes CP, Tye KM (2013): BLA to vHPC inputs modulate anxiety-related behaviors. *Neuron*. 79:658-664.

65. Nguyen R, Koukoutselos K, Forro T, Ciocchi S (2023): Fear extinction relies on ventral hippocampal safety codes shaped by the amygdala. *Sci Adv*. 9:eadg4881.

66. Mishra AK, Varma AR (2023): A Comprehensive Review of the Generalized Anxiety Disorder. *Cureus J Med Science*. 15.

67. Bredemeier K, Berenbaum H (2020): Perceptions of Threat. *Generalized Anxiety Disorder and Worrying*, pp 25-42.

68. McHugo M, Talati P, Armstrong K, Vandekar SN, Blackford JU, Woodward ND, et al. (2019): Hyperactivity and Reduced Activation of Anterior Hippocampus in Early Psychosis. *Am J Psychiatry*. 176:1030-1038.

69. Wolff AR, Bygrave AM, Sanderson DJ, Boyden ES, Bannerman DM, Kullmann DM, et al. (2018): Optogenetic induction of the schizophrenia-related endophenotype of ventral hippocampal hyperactivity causes rodent correlates of positive and cognitive symptoms. *Sci Rep*. 8:12871.

70. Navidhamidi M, Ghasemi M, Mehranfard N (2017): Epilepsy-associated alterations in hippocampal excitability. *Rev Neuroscience*. 28:307-334.

Supplementary Figures

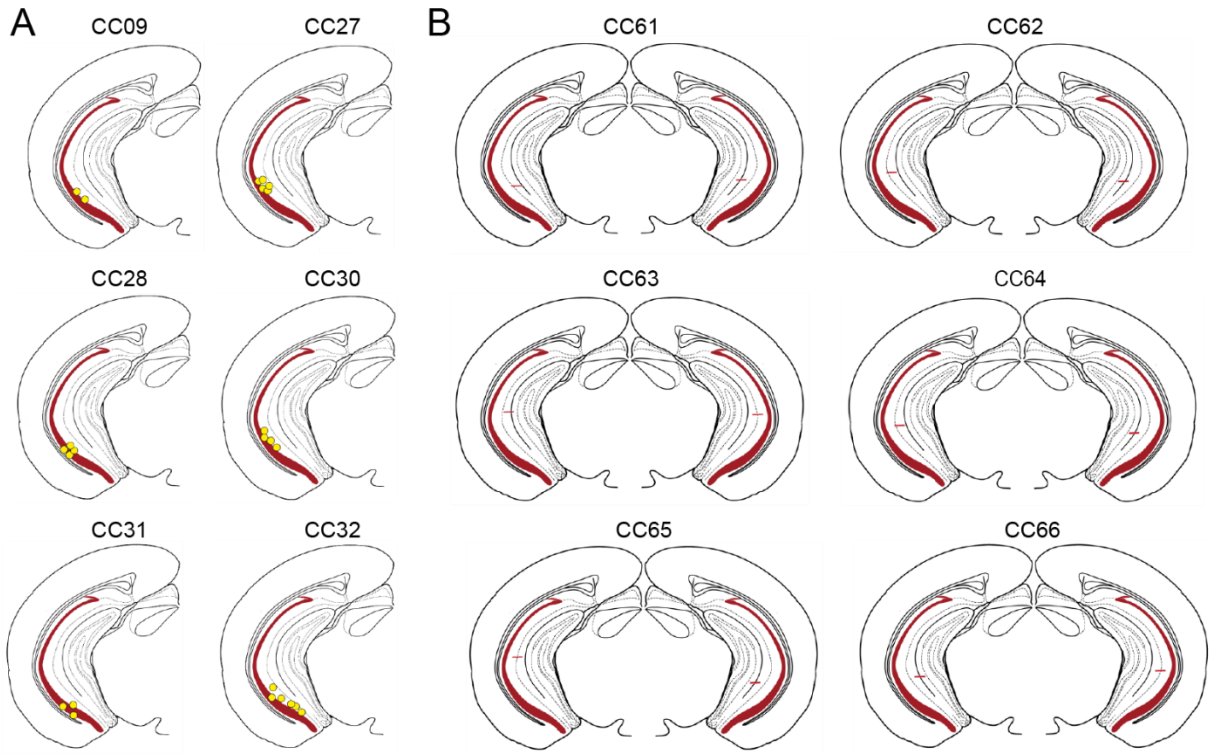

Suppl. Figure 1. (A) Schematic representation of tetrode recordings sites indicated by electrolytic lesions (yellow circles). **(B)** Schematic representation of optic fiber implants (red lines). Identifying animal names are on top of every schematic representation.

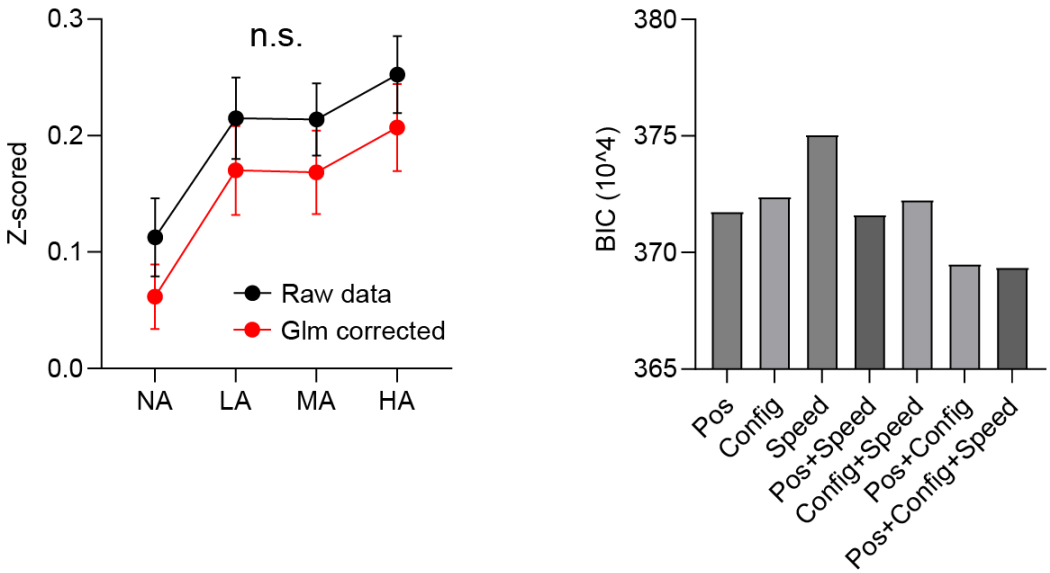

Suppl. Figure 2. Left, Z-scored firing rate activity of the overall recorded population and GLM corrected values for speed-modulated neurons. Two-way RM ANOVA Interaction values: F = 0.01, p = 0.999. All post hoc test results in supplementary table 15. Right, Seven different GLMs fitted with different combinations of variables (Position, Speed, Conflict) and their goodness-of-fit compared using the BIC criterion. Note that the speed variable alone was poorly predictive of the firing rates of neurons.

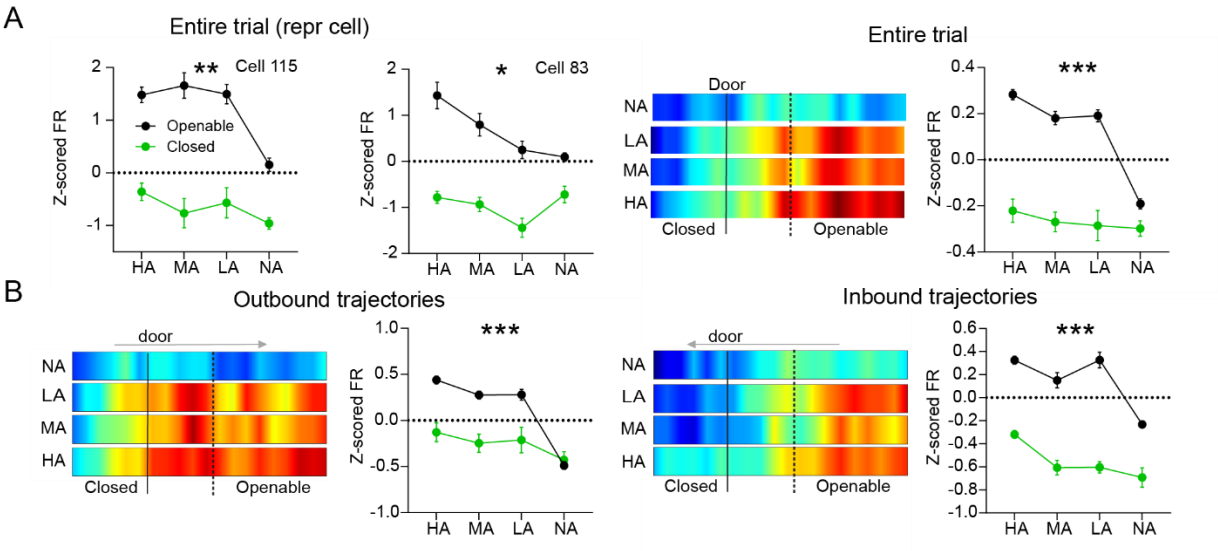

Suppl. Figure 3. Scaling of vH activity in 'descending' anxiety configurations. (A) Left, individual example neurons with decreasing Z-scored activity in the open across anxiety levels (Cell 115: Two-way RM ANOVA Interaction values: F = 5.24, p = 0.004, r = -0.0931 and p = 0.696 for closed and r = -0.686 and p < 0.001 for open, Spearman correlation. Cell 83: Two-way RM ANOVA Interaction values: F = 4.24, p = 0.012, r = -0.38 and p = 0.098 for closed and r = -0.55 and p < 0.001 for open, Spearman correlation. All post hoc test results in supplementary table 16 and supplementary table 17). Right, heatmaps and Z-scored firing rates show vH population activity progressively decreasing in the open part compared to the closed part (Two-way RM ANOVA Interaction values: F = 30.23, p < 0.001. All post hoc test results in supplementary table 18, r = -0.24 and p = 0.3 for closed and r = -0.77 and p < 0.001 for open, Spearman correlation. Heat maps depict the linearized firing rate activity of the entire recorded population (n = 207, N = 6 animals, n = 22 experimental days). **(B)** Heatmaps and Z-scored firing rates separated into outbound (left) and inbound trajectories (right) showing gradual scaling during outbound and switching of activity respectively. Left, Two-way RM ANOVA Interaction values: F = 34.15, p < 0.001, r = -0.4 and p = 0.078 for closed and r = -0.72 and p < 0.001, Spearman correlation. Right, two-way RM ANOVA Interaction values: F = 7.61, p < 0.001, r = -0.628 and p = 0.003 for closed and r = -0.548 and p < 0.001, Spearman correlation. All post hoc test results in supplementary table 19 and supplementary table 20. N = 207 cells, n = 8615 trials. Error bars represent ± SEM.

Supplementary Tables

Dunn's multiple comparisons test	Summary	Adjusted P Value
NA vs. LA	ns	0.613
NA vs. MA	ns	0.117
NA vs. HA	*	0.014
LA vs. MA	ns	>0.999
LA vs. HA	ns	0.967
MA vs. HA	ns	>0.999

Suppl table 1, referring to Figure 1B left.

Dunn's multiple comparisons test	Summary	Adjusted P Value
NA vs. LA	***	<0.001
NA vs. MA	***	<0.001
NA vs. HA	***	<0.001
LA vs. MA	ns	>0.999
LA vs. HA	ns	>0.999
MA vs. HA	ns	>0.999

Suppl table 2, referring to Figure 1B right.

Tukey's multiple comparisons test	Summary	Adjusted P Value
LA Ctr vs. Arch	ns	0.338
MA Ctr vs. Arch	*	0.044
HA Ctr vs. Arch	*	0.044
Ctr NA vs. LA	*	0.028

Ctr NA vs. MA	***	<0.001
Ctr NA vs. HA	***	<0.001
Ctr LA vs. MA	ns	0.693
Ctr LA vs. HA	ns	0.286
Ctr MA vs. HA	ns	0.451
Arch NA vs. LA	ns	0.571
Arch NA vs. MA	ns	0.730
Arch NA vs. HA	ns	0.259
Arch LA vs. MA	ns	0.921
Arch LA vs. HA	ns	0.976
Arch MA vs. HA	ns	0.624

Suppl table 3, referring to Figure 2D right.

Tukey's multiple comparisons test	Summary	Adjusted P Value
NA Openable vs. Closed	*	0.030
LA Openable vs. Closed	ns	0.957
MA Openable vs. Closed	***	<0.001
HA Openable vs. Closed	***	<0.001
Openable NA vs. LA	*	0.015
Openable NA vs. MA	***	<0.001
Openable NA vs. HA	***	<0.001
Openable LA vs. MA	***	<0.001
Openable LA vs. HA	***	<0.001
Openable MA vs. HA	ns	0.088
Closed NA vs. LA	ns	0.162
Closed NA vs. MA	ns	0.123

Closed NA vs. HA	ns	0.052
Closed LA vs. MA	ns	0.817
Closed LA vs. HA	ns	0.668
Closed MA vs. HA	ns	0.997

Suppl table 4, referring to Figure 3A left.

Tukey's multiple comparisons test	Summary	Adjusted P Value
NA Openable vs. Closed	ns	0.125
LA Openable vs. Closed	***	<0.001
MA Openable vs. Closed	**	0.004
HA Openable vs. Closed	***	<0.001
Openable NA vs. LA	**	0.008
Openable NA vs. MA	ns	0.078
Openable NA vs. HA	***	<0.001
Openable LA vs. MA	ns	0.998
Openable LA vs. HA	ns	0.109
Openable MA vs. HA	ns	0.351
Closed NA vs. LA	ns	0.997
Closed NA vs. MA	ns	0.171
Closed NA vs. HA	ns	0.902
Closed LA vs. MA	ns	0.079
Closed LA vs. HA	ns	0.816
Closed MA vs. HA	ns	0.303

Suppl table 5, referring to Figure 3A middle.

Tukey's multiple comparisons test	Summary	Adjusted P Value
NA Openable vs. Closed	ns	0.094
LA Openable vs. Closed	***	<0.001
MA Openable vs. Closed	***	<0.001
HA Openable vs. Closed	***	<0.001
Openable NA vs. LA	***	<0.001
Openable NA vs. MA	**	0.004
Openable NA vs. HA	***	<0.001
Openable LA vs. MA	ns	0.886
Openable LA vs. HA	ns	0.165
Openable MA vs. HA	ns	0.820
Closed NA vs. LA	ns	0.101
Closed NA vs. MA	ns	0.078
Closed NA vs. HA	ns	0.125
Closed LA vs. MA	ns	0.929
Closed LA vs. HA	ns	0.971
Closed MA vs. HA	ns	0.996

Suppl table 6, referring to Figure 3A right.

Tukey's multiple comparisons test	Summary	Adjusted P Value
NA Openable vs. Closed	ns	0.678
LA Openable vs. Closed	ns	0.217
MA Openable vs. Closed	**	0.003
HA Openable vs. Closed	*	0.013
Openable NA vs. LA	**	0.007

Openable NA vs. MA	***	<0.001
Openable NA vs. HA	***	<0.001
Openable LA vs. MA	***	<0.001
Openable LA vs. HA	*	0.018
Openable MA vs. HA	ns	0.605
Closed NA vs. LA	ns	0.421
Closed NA vs. MA	ns	0.998
Closed NA vs. HA	ns	0.781
Closed LA vs. MA	ns	0.461
Closed LA vs. HA	ns	0.779
Closed MA vs. HA	ns	0.722

Suppl table 7, referring to Figure 3B left.

Tukey's multiple comparisons test	Summary	Adjusted P Value
NA Openable vs. Closed	***	<0.001
LA Openable vs. Closed	***	<0.001
MA Openable vs. Closed	***	<0.001
HA Openable vs. Closed	***	<0.001
Openable NA vs. LA	**	0.002
Openable NA vs. MA	ns	0.073
Openable NA vs. HA	**	0.004
Openable LA vs. MA	ns	0.976
Openable LA vs. HA	ns	0.964
Openable MA vs. HA	ns	>0.999
Closed NA vs. LA	ns	0.073
Closed NA vs. MA	**	0.009

Closed NA vs. HA	*	0.019
Closed LA vs. MA	ns	0.840
Closed LA vs. HA	ns	0.999
Closed MA vs. HA	ns	0.210

Suppl table 8, referring to Figure 3B right.

Tukey's multiple comparisons test	Summary	Adjusted P Value
NA vs. LA	***	<0.001
NA vs. MA	***	<0.001
NA vs. HA	***	<0.001
LA vs. MA	ns	0.275
LA vs. HA	**	0.010
MA vs. HA	ns	0.175

Suppl table 9, referring to Figure 4A.

Tukey's multiple comparisons test	Summary	Adjusted P Value
NA vs. LA	***	<0.001
NA vs. MA	**	0.009
NA vs. HA	***	<0.001
LA vs. MA	ns	0.121
LA vs. HA	ns	>0.999
MA vs. HA	ns	0.213

Suppl table 10, referring to Figure 4C top.

Tukey's multiple comparisons test	Summary	Adjusted P Value
LA vs. MA	**	0.004
NA vs. LA	ns	0.359
NA vs. MA	ns	0.115
NA vs. HA	ns	0.260
LA vs. HA	**	0.002
MA vs. HA	ns	0.706

Suppl table 11, referring to Figure 4C middle.

Tukey's multiple comparisons test	Summary	Adjusted P Value
MA vs. HA	ns	0.051
NA vs. LA	ns	0.720
NA vs. MA	ns	0.967
NA vs. HA	*	0.023
LA vs. MA	ns	0.933
LA vs. HA	*	0.021

Suppl table 12, referring to Figure 4C bottom.

Uncorrected Fisher's LSD	Summary	Individual P Value
Ctr Closed vs. Openable	**	0.002
Nov Closed vs. Openable	ns	0.070
Closed Ctr vs. Nov	ns	0.372
Openable Ctr vs. Nov	ns	0.373

Suppl table 13, referring to Figure 5C.

Dunn's multiple comparisons test	Summary	Adjusted P Value
NA vs. LA	ns	0.239
NA vs. MA	**	0.002
NA vs. HA	***	<0.001
LA vs. MA	ns	0.683
LA vs. HA	**	0.002
MA vs. HA	ns	0.239

Suppl table 14, referring to Figure 6B.

Tukey's multiple comparisons test	Summary	Adjusted P Value
NA Raw data vs. GLM corrected	ns	0.241
LA Raw data vs. GLM corrected	ns	0.386
MA Raw data vs. GLM corrected	ns	0.336
HA Raw data vs. GLM corrected	ns	0.362

Suppl table 15, referring to Supplementary figure 2 left.

Tukey's multiple comparisons test	Summary	Adjusted P Value
HA Openable vs. Closed	***	<0.001
MA Openable vs. Closed	***	<0.001
LA Openable vs. Closed	***	<0.001

NA Openable vs. Closed	***	<0.001
Openable HA vs. MA	ns	0.747
Openable HA vs. LA	ns	>0.999
Openable HA vs. NA	**	0.001
Openable MA vs. LA	ns	0.907
Openable MA vs. NA	**	0.003
Openable LA vs. NA	**	0.001
Closed HA vs. MA	ns	0.370
Closed HA vs. LA	ns	0.722
Closed HA vs. NA	*	0.036
Closed MA vs. LA	ns	0.328
Closed MA vs. NA	ns	0.758
Closed LA vs. NA	ns	0.291

Suppl table 16, referring to Supplementary figure 3A left.

Tukey's multiple comparisons test	Summary	Adjusted P Value
HA Openable vs. Closed	***	<0.001
MA Openable vs. Closed	***	<0.001
LA Openable vs. Closed	***	<0.001
NA Openable vs. Closed	**	0.007
Openable HA vs. MA	ns	0.247
Openable HA vs. LA	*	0.021
Openable HA vs. NA	*	0.014
Openable MA vs. LA	ns	0.140
Openable MA vs. NA	ns	0.170
Openable LA vs. NA	ns	0.879

Closed HA vs. MA	ns	0.710
Closed HA vs. LA	*	0.045
Closed HA vs. NA	ns	0.952
Closed MA vs. LA	ns	0.195
Closed MA vs. NA	ns	0.632
Closed LA vs. NA	**	0.002

Suppl table 17, referring to Supplementary figure 3A middle.

Tukey's multiple comparisons test	Summary	Adjusted P Value
HA Openable vs. Closed	***	<0.001
MA Openable vs. Closed	***	<0.001
LA Openable vs. Closed	***	<0.001
NA Openable vs. Closed	*	0.029
Openable HA vs. MA	*	0.017
Openable HA vs. LA	*	0.019
Openable HA vs. NA	***	<0.001
Openable MA vs. LA	ns	0.951
Openable MA vs. NA	***	<0.001
Openable LA vs. NA	***	<0.001
Closed HA vs. MA	ns	0.499
Closed HA vs. LA	ns	0.131
Closed HA vs. NA	ns	0.276
Closed MA vs. LA	ns	0.961
Closed MA vs. NA	ns	0.170
Closed LA vs. NA	ns	0.988

Suppl table 18, referring to Supplementary figure 3A right.

Tukey's multiple comparisons test	Summary	Adjusted P Value
HA Openable vs. Closed	**	0.003
MA Openable vs. Closed	**	0.004
LA Openable vs. Closed	*	0.020
NA Openable vs. Closed	ns	0.558
Openable HA vs. MA	*	0.014
Openable HA vs. LA	ns	0.066
Openable HA vs. NA	***	<0.001
Openable MA vs. LA	ns	>0.999
Openable MA vs. NA	***	<0.001
Openable LA vs. NA	***	<0.001
Closed HA vs. MA	ns	0.185
Closed HA vs. LA	ns	0.311
Closed HA vs. NA	**	0.001
Closed MA vs. LA	ns	0.960
Closed MA vs. NA	*	0.031
Closed LA vs. NA	ns	0.077

Suppl table 19, referring to Supplementary figure 3B left.

Tukey's multiple comparisons test	Summary	Adjusted P Value
HA Openable vs. Closed	***	<0.001
MA Openable vs. Closed	***	<0.001
LA Openable vs. Closed	***	<0.001
NA Openable vs. Closed	**	0.004

Openable HA vs. MA	*	0.011
Openable HA vs. LA	ns	>0.999
Openable HA vs. NA	***	<0.001
Openable MA vs. LA	**	0.005
Openable MA vs. NA	**	0.006
Openable LA vs. NA	***	0.001
Closed HA vs. MA	ns	0.085
Closed HA vs. LA	*	0.028
Closed HA vs. NA	*	0.017
Closed MA vs. LA	ns	>0.999
Closed MA vs. NA	ns	0.906
Closed LA vs. NA	ns	0.777

Suppl table 20, referring to Supplementary figure 3B right.